Int. J. Electrochem. Sci., 10 **(2015)** 1752 - 1761

International Journal of
ELECTROCHEMICAL
SCIENCE
www.electrochemsci.org

Short Communication

Effect of Annealing Temperature on Structural, Morphology and Optical Properties of ZnO Nano-Needles Prepared by Zinc-Air Cell System Method

T.D Malevu[*], *R.O Ocaya*

Department of Physics, University of the Free State (QwaQwa Campus), P. Bag X13, Phuthaditjhaba 9866.
[*]E-mail: MalevuTD@qwa.ufs.ac.za

Received: 17 November 2014 / *Accepted:* 22 December 2014 / *Published:* 30 December 2014

ZnO nano-needles have been synthesized successfully on zinc substrate with the zinc-air cell method at room temperature. The effect of annealing temperature on the structure, morphology and optical properties of ZnO nano-needles were investigated using X-ray diffraction (XRD), Field Emission Scanning electron microscopy (FE-SEM) and ultraviolet-visible spectrometry (UV-Vis) techniques. XRD measurements indicated the presence of ZnO nano-needles with a hexagonal wurtzite structure and no external impurities. As the annealing temperature was increased from 400^{o}C to 600^{o}C the particle size increased and the nano-needles became more orientated with average height between 538.1 nm to 1195 nm. The UV-Vis measurements showed a slight decrease in absorbance and the absorption edge shifted slightly to lower energy. The apparent increase in the band gap energy from 3.29 to 3.30eV over the 400-600^{o}C temperature range is a variation of within 2% in the range, and cannot reliably be attributed to adverse effects such as defect formation at the high temperatures since it is within the measurement uncertainty. The nano-needles exhibit strong absorption peaks, which decrease with annealing temperature, in the wavelength range of ~360nm to 380nm. The nano-structures also exhibited increased crystallization strength. The absence of impurities after annealing was confirmed using energy dispersive spectroscopy

Keywords: Zinc oxide, nano-needles, zinc air system, annealing

1. INTRODUCTION

Over the past decades Zinc Oxide (ZnO) has drawn much research attention due to its unique properties. For instance, it has wide band gap energy of 3.37eV and a large exciton binding energy of 60 meV [1-3]. It has good transparency, high electron mobility of ~2000 cm^2/(V·s) at 80 K [2] and it is arguably the richest single semiconductor material in terms of variety of one-dimensional (1-D) nanostructures such as nano-rods, nano-flakes and nano-needles [3-6]. These properties make this

material a potential candidate in many different optoelectronic applications such as solar cells, wave guides, laser diodes and gas sensors [7, 8]. The properties of ZnO nanostructures are interesting because they differ substantially from those of bulk ZnO. Different methods are currently employed to synthesize ZnO nanostructures. Some examples of these methods are the sol-gel, hydrothermal, chemical bath deposition (CBD) electro-deposition, microwave-assisted techniques, chemical vapor deposition (CVD) and precipitation methods [9-14]. The authors have reported the successful synthesis of ZnO nano-needles on a zinc plate using a novel, exploratory concept using a zinc-air cell system (ZAC) [22]. This method is environmentally friendly, uses low temperature and low cost material such as steel wool, zinc plate, recycled void paper, low discharging resistor and oxygen derived from the atmosphere. XRD studies have shown that this method allows different nanostructures to be obtained depending on the parameter of variation such as discharge time and type of electrolyte used. In this paper, we report the effect of annealing temperature on the samples synthesized over one hour discharging time using the ZAC system. There is evidence in the literature to suggest that annealing at high temperature potentially plays a number of roles. It is reported that ZnO nanostructures synthesized at room temperatures remain stable even at very high temperatures [13, 14]. ZnO nano-structures continue to exhibit a usable, wide band gap of ~3.13eV, a decrease of approximately only 7% of its room temperature band gap at a temperature of 1100^{o}C [14]. This has a promising significance for future semiconductor devices at high temperatures that are comparable to compound semiconductors like silicon carbide with band gap energy of 3.23eV [15]. High temperature annealing of ZnO nano-structures also appears to increase optical properties such as photoluminescence [16], improved crystallinity [17]. Furthermore, annealing at higher temperatures provides a mechanism for the substitution of a zinc atom in the presence of an impurity in a process that is effectively akin to doping ZnO [18]. However, it has also been reported by Hwang et al [19] that annealing resulted in the deterioration of the photoluminescence spectra of ZnO nano-structures when deposited on soda-lime-silica glass substrates. In this article the substrate is predominantly zinc. Chin et al [20] have reported an increase in the intensity of the ultraviolet (UV) emission intensity with annealing temperature and dwelling time, in addition to increased crystallization [20, 23]. In this paper the effect of annealing temperature on the structure, morphology and optical properties of the ZAC synthesized ZnO nano-needles was investigated. The primary aim of the investigation was to evaluate the effect of temperature on the stability of nano-needles particularly for the use of the nano-needle structures for wide band gap, high temperature devices such as LEDs and a variety of other sensing devices.

2. EXPERIMENTAL

2.1. Synthesis of ZnO nano-needles

Solutions of pure sodium hydroxide of 2M concentration were prepared in distilled water using commercial sodium hydroxide pellets CP from Associated Chemical Enterprises (Pty) Ltd. A homogeneously mixed solution was obtained under constant magnetic stirring at room temperature. The solutions were then cooled to room temperature before being injected into the cell enclosure containing large area of pure zinc (purity of 99.9% by mass) and air cathode composed of steel wool

and recycled void paper to allow the transfer of electrons from the anode to the cathode. The system was then allowed to discharge over one hour into a 470Ω resistor. After the discharge, the zinc plate was removed and cut into several 1x1cm^2 pieces before annealing. The pieces were placed into an alumina boat that was put in a box-type furnace. The heating was done at different temperatures 400^{o}C, 450^{o}C, 500^{o}C and 600^{o}C for 60mins. Annealing time is known to affect the extent to crystallization [10, 16]. The samples were then allowed to cool down naturally back to room temperature prior to characterization.

2.2. Characterization

The structure of ZnO nano-needles was determined using X-ray diffraction (XRD, Bruker AXS D8 Advanced) with CuKα radiation of 1.5418Å wavelength. The particle morphology and chemical composition of the samples were then studied using a Joel JSM-9800F Field Emission Scanning electron microscope (FE-SEM) equipped with a dispersive x-ray spectrometer (EDS). The optical properties were studied using a Perkin-Elmer Lambda 950 UV-Vis spectrometer.

3. RESULTS AND DISCUSSION

3.1. Structural characterization

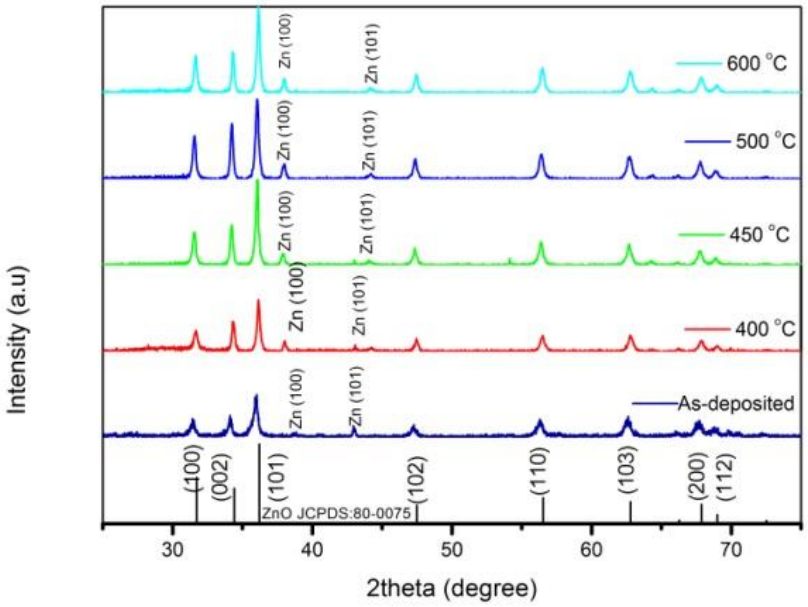

Figure 1. XRD pattern of ZnO nanostructures synthesized at different temperatures

Figure 1 shows the XRD patterns of ZnO nano-needles synthesized at different concentrations. The diffraction peaks at scattering angle (2θ) of 31.8^o, 34.4^o, 36.3^o, 47.5^o, 56.5^o, 62.7^o, 66.3^o, 67.9^o and 69.0^o correspond to the reflections from (100), (002), (101), (102), (110), (103), (200), (112) and (200)

crystal planes respectively. These reflections correspond to the standard card (JCPDS: 80-0075) of the hexagonal wurtzite ZnO structure. The other prominent diffraction peaks in the figure are attributed to zinc, confirmed with the JCPDS: 04-0831 standard card of hexagonal structured zinc. No impurities were observed. **Figure 3.** Effect of temperature on intensityFigure 3 suggests that as the temperature increases the diffraction peaks are narrower and exhibit a higher intensity, which further suggests that the nano-needles become more crystalline. This can be attributed to the change in crystal size. The major peaks were then used to estimate the ZnO nano-needles particle sizes according to the Debye-Scherrer equation:

$$D = \frac{k\lambda}{\beta \cos \theta}, \quad (1)$$

where D is the size of the crystallites, β is the full-width at half-maximum (HWHM) of a diffraction line located at angle θ, λ is the x-ray wavelength and k is a Scherrer constant (0.9), which depends on the peak breadth, crystallite shape, and crystallite size distribution. The crystallite sizes were found to be increasing with increasing temperature as shown in Figure 2, the average particle size was found to be ~25.56 nm. Thus temperature plays an important role in tuning the material crystal sizes.

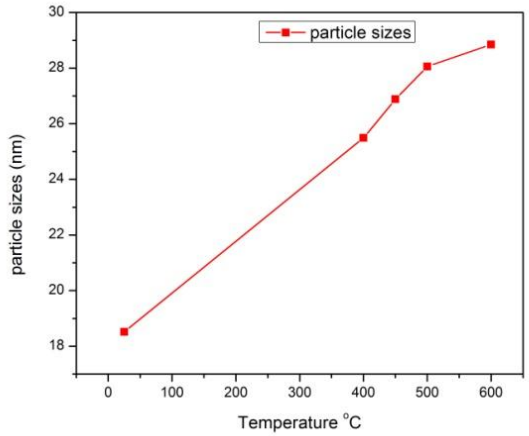

Figure 2. Effect of temperature on particle size

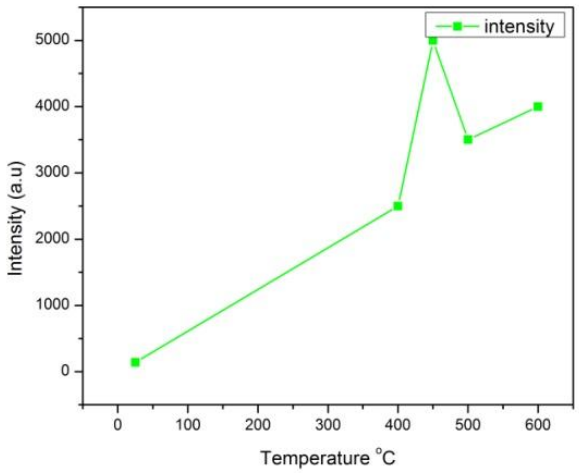

Figure 3. Effect of temperature on intensity

The lattice parameters of ZnO thin films annealed at different temperatures were calculated using Miller indices *hkl* (equation 2) according to the following equation

$$\left(\frac{1}{d_{hkl}}\right)^2 = \frac{4}{3} + \left(\frac{h^2+h^2+hk}{a^2}\right) + \frac{l^2}{c^2} \quad (2)$$

where a and c are the lattice constants. The lattice parameters calculated at first order diffraction are a = 3:2498 Å and c = 5:2066 Å and are consistent with the JCPDS: 80-0075 standard card. The lattice parameters were estimated at first order reflection ($n = 1$) on the (100) plane using

$$a = \frac{\lambda}{\sqrt{3}\ \sin\theta} \approx 0.327 \pm 0.02 \text{ nm} \quad (3)$$

and

$$c = \frac{\lambda}{\sin\theta} \approx 0.5662 \pm 0.02 \text{ nm} \quad (4)$$

Table 1 shows the variation of lattice parameter a *and* c with the annealing temperature. The table shows a decrease in lattice parameters (a) and (c) with increasing temperature.

Table 1. Effect of annealing temperature on lattice parameters

Annealing temperature (^{o}C)	2θ (degrees)	Lattice constant, *c* (Å)	Lattice constant, *a* (Å)
25	31.4316	5.686	3.283
400	31.6567	5.666	3.271
450	31.5413	5.664	3.270
500	31.5543	5.649	3.261
600	31.6406	5.646	3.260

The results of Ivetić et al also depict a general reduction in both lattice parameters when the temperature is increased from 700^{o}C to 1100^{o}C although their work considers the effect of a magnesium impurity atom substituting a zinc atom at a higher temperature. The radius of the magnesium atom is smaller than that of a zinc atom and this explains the reduction of the lattice parameters. In this particular case the lowering of lattice parameters is thought to be the effect of stress undergone by thin film grains and may be due to a change in the nature and concentration of the native imperfections [24]. This causes compression of the lattice parameters. ZnO nanostructures may typically have a number of defects such as oxygen vacancies, lattice disorders, etc. As a result of annealing these defects are removed and the lattice contracts. Also lattice relaxation due to dangling bonds should be taken into account. The dangling bonds on ZnO surface interact with oxygen ions from the atmosphere and due to electrostatic attraction, leading to a lattice that is slightly contracted [24, 25].

3.2. Surface and chemical composition characterization

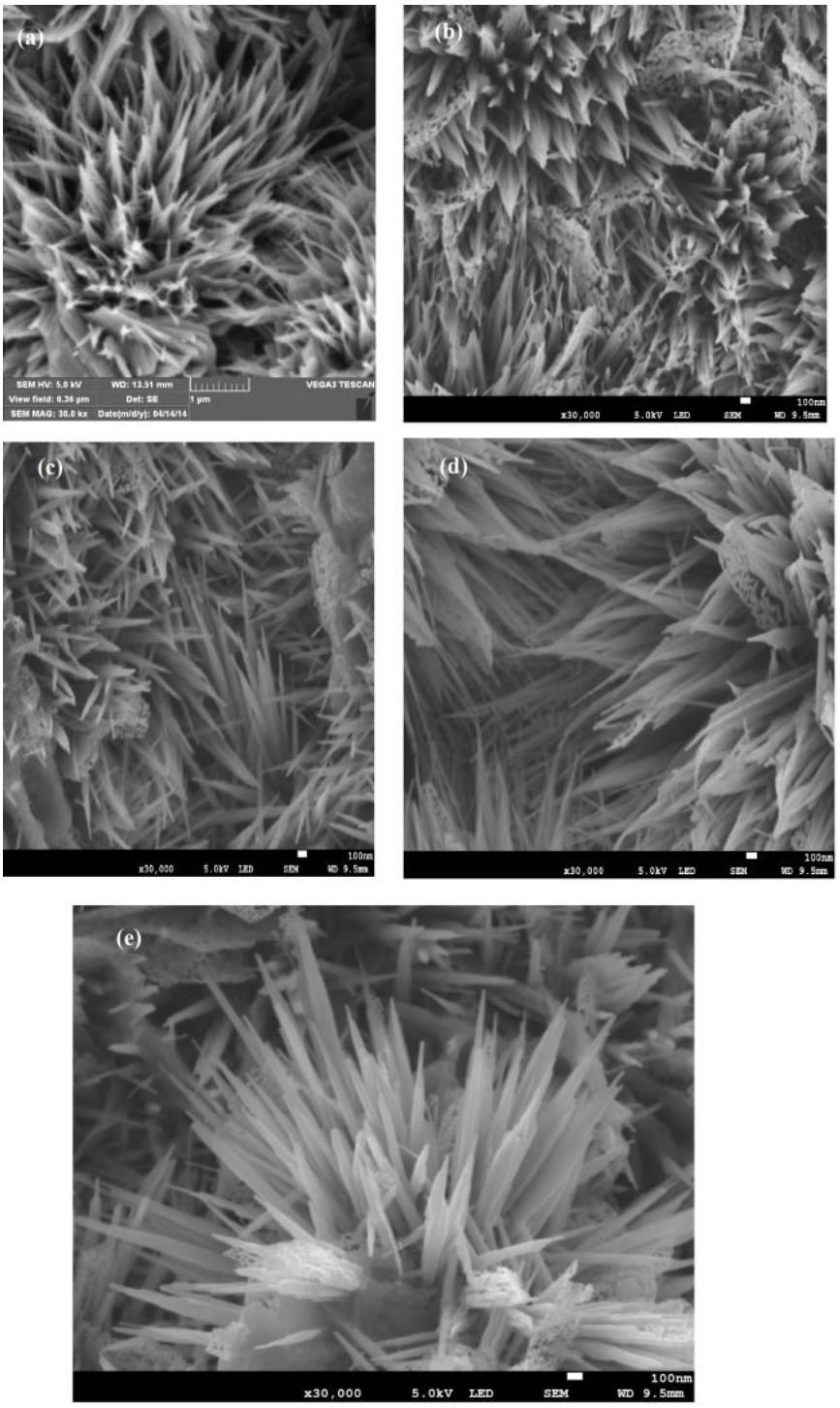

Figure 4. SEM micrographs of ZnO nano-needles before and after annealed at different temperatures: (a) as-deposited (b) 400 ^{o}C (c) 450 ^{o}C (d) 500 ^{o}C and (e) 600 ^{o}C.

Figure 4(a)-(e) show the FE-SEM micrographs of ZnO nano-needles synthesized at different temperatures ranging from room temperature to 600^{o}C. It is observed in all the images that the grown nano-needles are randomly orientated with the preferred vertical orientation. As the temperature

increases, the nano-needles appear to be tapered to a sharper end at the top. Therefore the major peaks were taken to estimate the nano-needles length. The nano-needle lengths are in the range of 538.1 nm to 1195 nm.

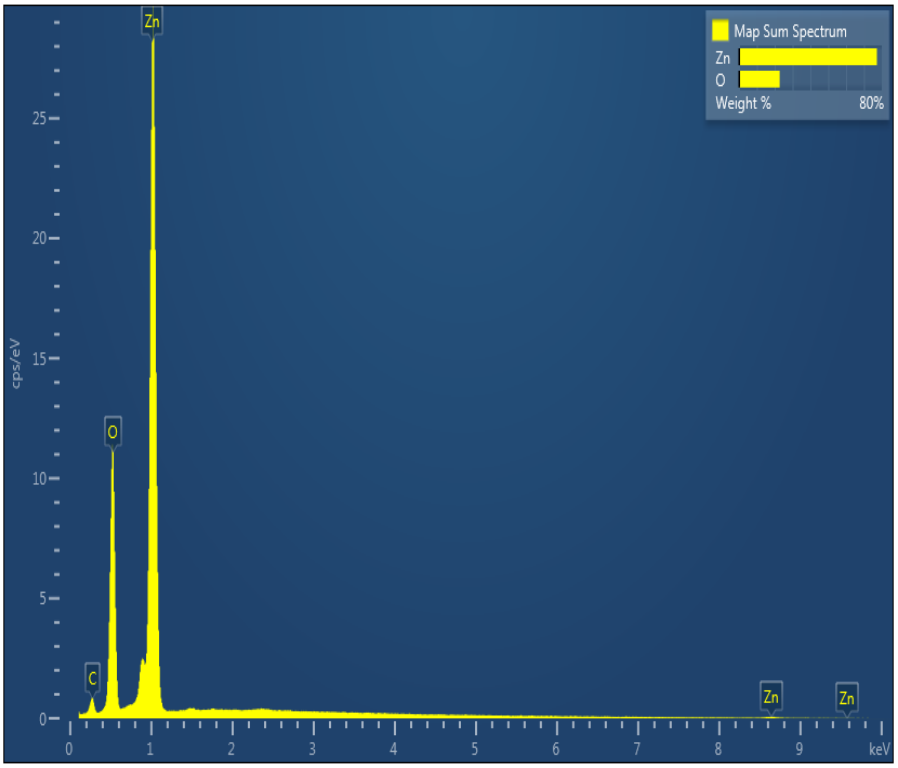

Figure 5. Chemical compositions of ZnO nano-needles

This indicates the presence of nano-needles that are suitable for optoelectronic applications such as solar cells, wave guides, laser diodes and gas sensors and field emitters [27, 28]. Figure 5 shows EDS spectrum measurements of the ZnO nano-needles. It is clear that there are no impurities from other materials besides carbon which can be attributed to either the handling of the sample or as a result of post heating. However, in spite of the EDS spectrum showing three peaks i.e. zinc, oxygen and carbon, the weight percent of Zn, and O elements obtained from EDS is nearly stoichiometric.

3.3. Band gap estimation using UV-VIS spectrometer

Figure 6 shows the UV-Vis spectra of ZnO nano-needles synthesized at different annealing temperatures. The ZnO nano-needles exhibit strong absorption peaks in the range of ~360nm to 380nm, which is attributed to the electronic transition of electrons from valence band to conduction band. This implies that ZnO nano-needles are in the regime of spatial excitonic confinement compared to bulk of ZnO. It is observed from the spectra that the absorbance of the samples decreases slightly with increase in annealing temperature and the absorption edge slightly shift lower energy. The red

shift of the absorption peak could be due to the changes in band gap as a function of annealing temperature.

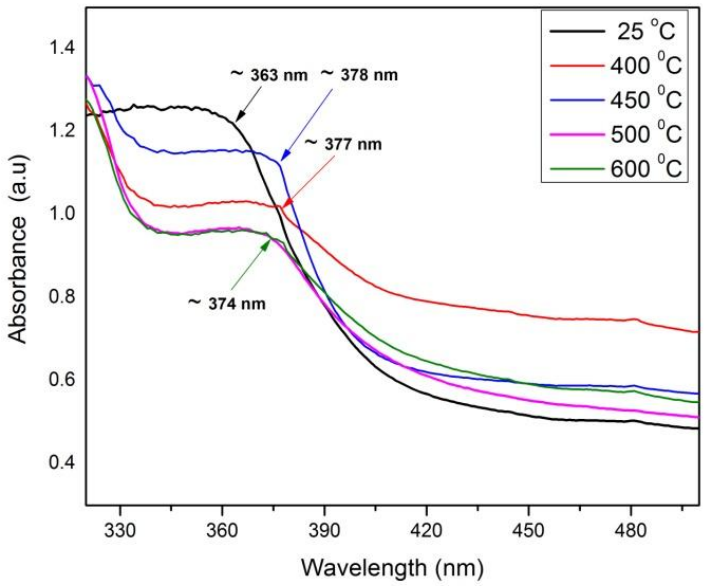

Figure 6. UV-Vis absorbance spectra of ZnO nano-needles synthesized at different annealing temperatures

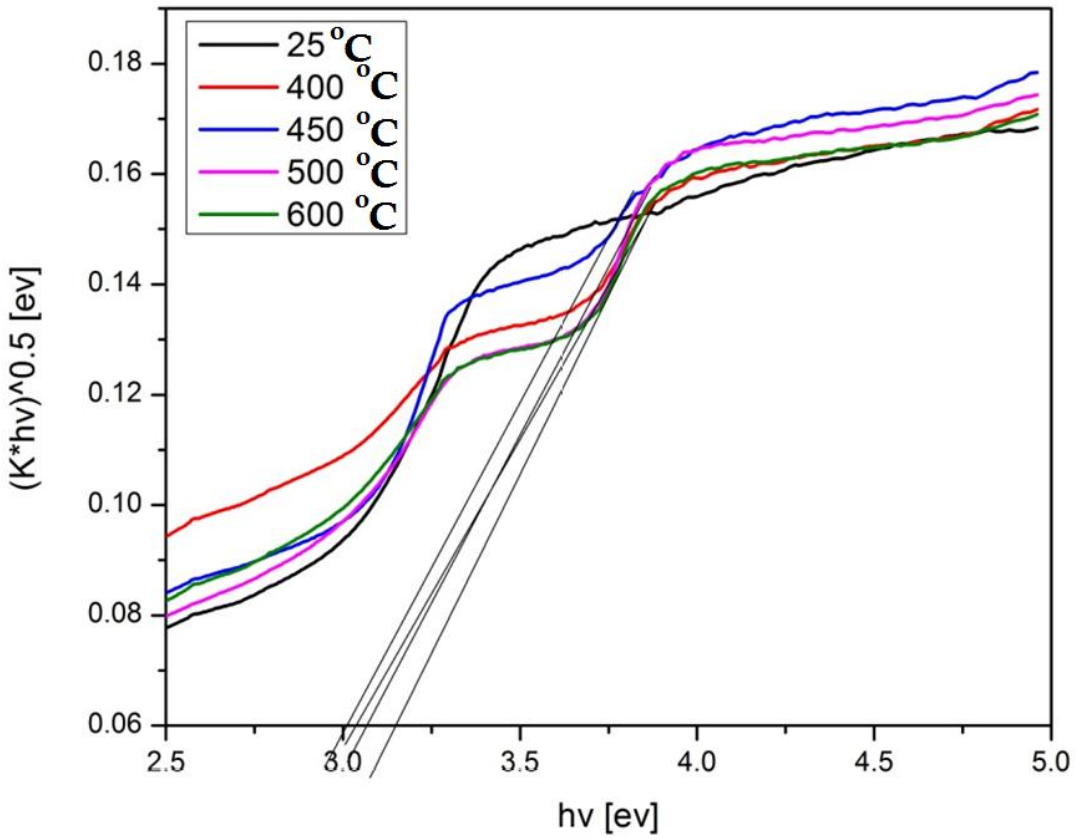

Figure 7. Plot of $(F(R)hv)^{0.5}$ as a function of photon energy (hv) of ZnO nano-needles.

The optical absorption of direct band gap ZnO nano-needles was estimated using the Kubelka–Munk function in Equation (5) and Tauc's relation, Equation (6) [26].

$$F(R) = \frac{(1-R)^2}{2R} \quad (5)$$

and

$$hv = (F(R) \times hv)^n, \quad (6)$$

where R is absolute reflectance of the sample layer, hv is photon energy ($h =$ Planck's constant and $v =$ frequency of the photon) and $n = 0.5$ for a direct band gap semiconductor like ZnO. The optical band gap was determined by extrapolating the steep segment of the sliding curve in a plot of $(F(R) \times hv)^n$ versus photon energy as shown in Figure 7. The estimated band gap E_g was found to be 3.29, 3.28, 3.3 and 3.3eV for ZnO thin films annealed at 400, 450, 500 and 600^{o}C, respectively. It is observed that the band gap increases roughly with increase in annealing temperature, which is thought to be the formation of defects at higher temperatures as discussed by Bouhssira et al [29]. There are other factors that explain the increase in energy band gap. For instance the effect of O_2 absorption by the film and referred to as the Burstein-Moss (BM) process [29, 30]. Moustaghfir et al [30] have shown that defects such as O/Zn ratio increases with annealing temperature which leads to variations in the electronic properties. The average estimated optical band gap of ZnO nano-needles is ~3.316±0.05eV.

4. CONCLUSIONS

In this paper we report on the effect of annealing temperature on the structural, morphological and optical properties of synthesized ZnO thin films synthesized using a new method referred to as the zinc-air cell. The measurements were made using XRD, FE-SEM and UV-Vis techniques. XRD measurements indicated that the synthesized ZnO nano-needles exhibit the hexagonal wurtzite structure with no impurities. An increase in height was observed as an effect of annealing temperature. UV-Vis showed an increase in band-gap as increase in heating temperature, although the variation is well within the measurement uncertainty and cannot reliably be attributed to band gap variation with temperature. Therefore, this method is suitable for some important applications such as LEDs, UV photo detectors, sensing and for other optoelectronic devices.

ACKNOWLEDGEMENTS
The authors thank Mr. A.H. Wako for assistance with characterization, and the financial support of the National Nano-Science Postgraduate Teaching and Training Platform (NNPTTP) and University of the Free State.

References

1. X. Li and Y. Wang, *J. Alloys Compd,* 9 (2011) 5765–5768
2. V. Srikant and D.R, Clarke, *J. Appl. Phys,* 83 (1998), 5447-5451
3. E. Pyne, G.P. Sahoo, K. Bhui, H. Bar, P. Sarkar, S. Samanta, A. Maity and A. Misra, *Spectrochim. Acta, Part A*, 93 (2012) 100-105
4. P. Wagner and R. Helbig, *J. Phys. Chem. Solids,* 35 (1974) 327

5. T.Y. Kim, J.Y. Kim, S.H. Lee, H.W, Shim, S.H, Lee, E.K. Suh and K.S. Nahm, *Synth. Met*, 144 (2004) 61–68
6. P.K. Baviskar, P.R. Nikam, S.S. Gargote, A. Ennaoui, and B.R. Sankapal, *J. Alloys Compd*, 551 (2013) 233–242
7. S. Cho, *Trans. Elecr. Electron. Mater*, 10 (2009) 1-4
8. F.J. Sheini, J. Singh, O.N. Srivasatva, D.S. Joag and M.A. More, *Appl. Surf. Sci*, 256 (2010) 2110–2114
9. J.J. Dong, C.H. Zhen, H.Y. Hao, J. Xing, Z.L. Zhang and Z.Y. Zheng, *J. Nano Letters*, 8 (2013) 378
10. X.C. Chen, J.P. Zhou, H.Y. Wang, P.S. Xu and G.P. Pan, *Chines Phys B*, 20 (2011) 096102
11. S. Yilmaz, J. Supercond Nov Magn, 27 (2014) 1083-1089
12. T.T. Miao, D.X. Sun, Y.R. Guo, C. Li. Y.L. Ma. G.Z. Fang and Q.J. Pan, *J. Nano Letters*, 8 (2013) 431
13. S.K. Chong, C.F. Dee and S.A Rahman, *J. Nano Letters*, 8 (2013) 174
14. C. Xiang-Cun, Z. Jie-Ping, W. Hai-Yang, X, Peng-Shou and P. Guo-Qiang, *Chines Phys B*, 20 (2011) 096102: 1-3
15. T.B. Ivetić,, M.R. Dimitrievska, N.L. Finčur, Lj.R. Đačanin, I.O. Gúth, B.F. Abramović, and S.R. Lukić-Petrović, *Ceram. Int*, 40 (2014) 1545-1552
16. J. Yang, *Sensors*, 13 (2013) 2719-2734
17. V. Ghafouri, A. Ebrahimzad And M. Shariati, *SCI IRAN*, 20 (2013) 1039–1048
18. H.C. Wang, C.H. Liao, Y.L. Chueh, C.C. Lai, P.C. Chou and S.Y. Ting, *Opt Commu Optics*, 3 (2013), 295-306.
19. K.S. Hwang, Y.J. Lee and S. Hwangbo, *J Ceram Process Res*, 8 (2007) 305-311.
20. H.S. Chin and L.S. Chao, *J Nanomater*, 2013(2013) doi: 10.1155/2013/424953
21. C.K. Yap, W.C. Tan, S.S. Alias and A.A. Mohamad, *J. Alloy Compd*, 484 (2009) 934-938.
22. T.D. Malevu and R.O. Ocaya, *Int. J. Electrochem. Sci.*, 9 (2014) 8011-8023
23. M. Saleem, L. Fang, A. Wakeel, M. Rashad and C.Y. Kong, *World Journal of Condensed Matter Physics* 2 (2012) 10-15
24. A.B. Usseinov, E.A. Kotomin, A.T. Zhukovskii and J. Puans, *Thin Solid Films* 553 (2014) 38–42
25. J. Chang, A.Z. Muhammad, W. Wlodarski and E.R. Waclawik, *Sensors*, 13 (2013) 8445-8460
26. Y. Tak, K. Yong and C. Park, *J. Cryst. Growth* 285 (2005) 549-554
27. Z. Han, L. Lia, Y. Wu, H. Pan, S. Shen and J. Chen, *J. Hazard. Mater*, 217-218 (2012) 100-106
28. K. Kara, E.S.E. Tuzemen and R. Esen, *Turk J Phys* 38 (2014) 238-244
29. N. Bouhssira, S. Abed, E. Tomasella, J. Cellier, A. Mosbah, M.S. Aida, M. Jacquet, *Appl. Surf. Sci*. 252 (2006) 5594-5597
30. A. Moustaghfir, E. Tomasella, S. Ben Amor, M. Jacquet, J. Cellier, T. Sauvage, *Surf. Coat. Technol* 174-175 (2003) 193-196